RSC Advances




ROYAL SOCIETY OF CHEMISTRY

www.rsc.org/advances

# Greener Synthetic Route for Superparamagnetic and Luminescent $\alpha$-$Fe_2O_3$ Nanoparticles in Binary Mixtures of Ionic liquid and Ethylene glycol

Preet Shikha, B.S Randhawa*, Tejwant Singh Kang*

*Department of Chemistry, UGC−Centre for Advanced Studies−I, Guru Nanak Dev University, Amritsar-143005, India*

The $\alpha$-$Fe_2O_3$ nanoparticles have been synthesized by facile route employing inherently green binary mixtures of ionic liquid (IL), 1-ethyl-3-methyl imidazolium ethylsulphate, $[C_2mim][C_2OSO_3]$ and ethylene glycol, EG. A room temperature grinding of $Fe(NO)_3.9H_2O$ in given binary mixture in the presence of NaOH led to formation of amorphous particles, which on calcination, yielded $\alpha$-$Fe_2O_3$ nanoparticles (NPs). The obtained NPs have been characterized by various states of art techniques such as X-ray diffraction, Raman spectroscopy, UV-Vis and photoluminescence spectroscopy. The surface and morphological features of NPs have been investigated using scanning and transmission electron microscopy. The prepared NPs have shown weak ferromagnetic character with essence of superparamagnetism as probed by vibrating sample magnetometer (VSM) and Mössbauer spectroscopy. The composition of binary mixture of solvent has been found to affect the size, morphology and characteristic properties of prepared $\alpha$-$Fe_2O_3$ NPs.

**Keywords:** Ionic liquid, Photoluminescence, Superparamagnetism, Mössbauer spectroscopy

**Corresponding author. Tel.: +91-183-2258802-Ext-3207; Fax: +91-183-2258820.*
*E-mail addresses: tejwantsinghkang@gmail.com, balwinderrandhawa@gmail.com*

## 1. Introduction

In the field of nanotechnology, iron oxide nanoparticles (NPs) has attracted a lot of attention from scientific community due to their peculiar properties and potential applications such as in pigments [1], gas sensors [2], field effect transistors [3], photoelectrolysis reactors [4, 5], contrast reagents and drug delivery [6], magnetic storage [7], as photoanode for possible photo-electrochemical cell [8], and in catalysis [9] etc. Among various forms of iron oxide NPs, the most common forms, $\alpha$-$Fe_2O_3$ and $\gamma$-$Fe_2O_3$ NPs are the extensively employed in various technical applications. However, $\alpha$-$Fe_2O_3$ NPs has received significant attention due to its higher stability under ambient conditions, low cost and non-toxic nature [10]. To achieve the desired stability of these NPs with increased efficiency for respective applications, extensive efforts have been made for controlling the size and morphology of $\alpha$-$Fe_2O_3$ NPs. Numerous reports are available in literature regarding the synthesis of $\alpha$-$Fe_2O_3$ NPs with distinct shapes such as flower shaped $\alpha$-$Fe_2O_3$ with high surface area and showing adsorption property of heavy metal ions [11], nanotubes and nanorods with a diameter of 30-50 nm, polyhedral, plate, disc and needle shaped morphology, which showed shape dependent magnetic properties [12, 13], nanodiscs (50-60 nm) [14], nanocubes having an average size of 15 nm with shape dependent optical properties [15] and many more.

On the other hand, ionic liquids (ILs) are the salts which are liquid at or below 100 $^oC$ and possess an array of unique physico-chemical properties such as negligible vapor pressure, high solvating ability, large electrochemical window, high ionic conductivity and high decomposition temperature [16, 17]. Owing to their properties, ILs are attracting great interest from researchers around globe for diverse scientific processes. One such interest is to utilize ILs as solvents and soft templates for the preparation of a variety of nano-structured materials [18-22]. There are many reports regarding the preparation of hematite NPs employing ILs using a variety of processes. Zheng *et al*., [23] have synthesized $\alpha$-$Fe_2O_3$ NPs of varying size and morphology via IL assisted hydrothermal route, possessing a weak ferromagnetic character with a saturation magnetization less than 1 emu/g. Kim *et al*., have synthesized superparamagnetic $\alpha$-$Fe_2O_3$ NPs by thermal decomposition of $Fe(CO)_5$ in an IL, $[C_8mim][BF_4]$-DMF mixture solvent system [24]. He *et al*., have used hydrophobic IL comprising of iron containing ions for direct synthesis of

$\alpha$-$Fe_2O_3$ nanocubes by hydrothermal method and investigated their application towards photo-electrochemical sensing of glucose [25]. Zheng *et al*., have reported the ionothermal synthesis $\alpha$-$Fe_2O_3$ nanoplates possessing a weak ferromagnetic character [26] and in another report, porous plate like $\alpha$-$Fe_2O_3$ mesocrystals have been prepared by a controlled solvent evaporation process in the presence of IL, [$C_4$mim][Cl] [27]. Similarly, photocatalytically active $\alpha$-$Fe_2O_3$ hollow microspheres have been synthesized from iron containing IL, [$C_8$mim][$FeCl_4$] under solvothermal condition [28].

As discussed above, till date, a variety of effective methods have been tested for the preparation of $\alpha$-$Fe_2O_3$ NPs including conventional as well as IL assisted methods. Most of these methods require expensive apparatus, multistep procedures, a large amount of energy as well as time and a variety of organic solvents. Therefore the need of hour is to prepare nanomaterials conveniently and environmentally benign methods. Hydrolysis stable ILs are the best choice as relatively greener solvents. Further, ILs possesses low surface tension which can favor high nucleation [29]. Besides this, the electronic as well as stearic stabilization, extended hydrogen bonded network and high directional polarizability in ILs leads to extended ordering of nanoscale structures while preventing the aggregation of NPs [30]. Further the fine tuning of the characteristic properties of ILs by judicious choice of respective ions of IL adds to the uniqueness of these solvents. On the other hand, EG can also be considered as a relatively greener solvent as compared to that of volatile organic solvents at least in terms of non-volatility of EG at room temperature. Therefore, the binary mixtures of ILs with other solvents such as water or EG are expected to provide unique properties towards self-assembly of amphiphiles and synthesis of nanomaterials, which are not available either in IL or other solvents in bulk [31, 32]. In this regard, a few reports have been published concerned with the self-assembly of amphiphiles in binary mixture of IL, 1-ethyl-3-methyl imidazolium ethylsulphate, [$C_2$mim][$C_2OSO_3$] and water where composition dependent behavior has been observed.

Herein, we report a simple and facile method where simple grinding of metal salt in binary mixture of an IL, 1-ethyl-3-methylimidazolium ethylsulphate, [$C_2$mim][$C_2OSO_3$] and ethylene glycol, EG as a solvent yields $\alpha$-$Fe_2O_3$ NPs. The luminescent and ferromagnetic nature of formed $\alpha$-$Fe_2O_3$ NPs with an essence of

superparamagnetism have been found to be dependent on the relative amount of IL and EG in their binary mixture. The IL and EG acts as solvent as well as templating agent which prevents the agglomeration of prepared NPs. The effect of composition of IL and EG binary mixture on various physico-chemical properties such as structural, optical and magnetic properties of $\alpha$-$Fe_2O_3$ NPs have been discussed in detail. The novelty of the work lies in the fact that there is no report in literature for the synthesis of NPs, specifically $\alpha$-$Fe_2O_3$ utilizing inherently greener binary mixtures of $[C_2mim][C_2OSO_3]$ and EG where composition dependent behavior towards characteristic properties of $\alpha$-$Fe_2O_3$ is expected. Further the low temperature route without the use of any sophisticated instrument adds to the usefulness of the present work. The $\alpha$-$Fe_2O_3$ NPs thus obtained exhibit high saturation magnetization and negligible coercivity, thus showing superparamagnetism along with luminescence which can find place in diverse biomedical applications.

## 2. Experimental section

**2.1 Synthesis of $\alpha$-$Fe_2O_3$ nanoparticles:** Ferric nitrate nonahydrate ($Fe(NO)_3.9H_2O$), ethylene glycol (EG), 1-Ethyl-3-Methyl Imidazolium Ethylsulphate (IL) and NaOH were purchased from Sigma with purity >98%. In a typical synthesis, 2 mmol of $Fe(NO)_3.9H_2O$ and different compositions of binary mixture of 1-ethyl-3-methylimidazolium ethylsulphate (IL) and ethylene glycol (EG) were ground for 20 min in mortar to form a viscous liquid. Further 6 mmol of NaOH was added and the mixture was ground for another 20 min which transformed to a thick paste. The thick paste was heated at 90 $^oC$ for 24h to ensure the completeness of reaction. The procedure of synthesis is shown schematically in Scheme.1. The obtained products from different compositions of binary mixture was dried in air after being washed by water and then alcohol which was further heated at 500$^o$C for 4 hr to remove the organic part and to increase the crystallinity of NPs. The obtained products have been coded as $\alpha$Fe-0, $\alpha$Fe-25, $\alpha$Fe-50, $\alpha$Fe-75, $\alpha$Fe-100 where the number denotes the percentage of IL in IL-EG binary mixture.

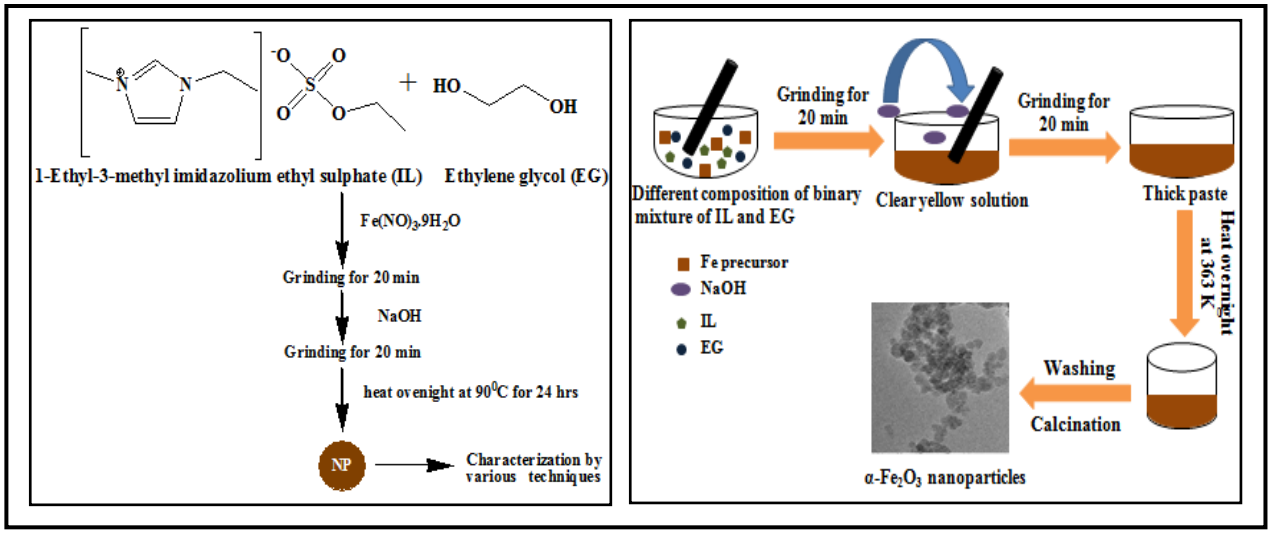


**Scheme.1.** Stepwise synthesis of $\alpha$-$Fe_2O_3$ NPs in binary mixture of IL and EG.

## 2.2 Characterization

X-ray diffractograms of the prepared nanoparticles (NPs) for phase analysis were recorded using a Rigaku Xpert Pro X-ray diffractometer provided with Cu K$\alpha$ radiation (1.541Å) in the 2θ range of $20^o$-$80^o$ at a step size of $0.02^o$. The average particle size was calculated based on XRD patterns using Scherrer's formula. Raman spectra were obtained for the prepared samples by placing the sample on a glass slide, using Renishaw Raman microscope equipped with 488 nm Ar-ion laser in the range of 100-2000 $cm^{-1}$. UV-Vis spectra were recorded on UV-spectrophotometer (UV-1800 SHIMADZU). Photoluminescence spectra were recorded on a Perkin Elmer spectrometer using the excitation wavelength of 390 and 450 nm at a slit width of 2.5 nm for both excitation and emission. Both UV-visible and photoluminescence measurements were carried out in dispersed form using ethanol as the solvent. The Mössbauer spectra of the NPs were measured using a conventional constant acceleration drive Mössbauer spectrometer with $^{57}$Co $\gamma$-ray source of 25 mCi embedded in rhodium matrix. The isomer shift values are reported with respect to pure iron absorber. Magnetic studies were carried out at room temperature in the applied magnetic field of -20 to +20 kOe using Microsense EV-90 vibrating sample magnetometer. The surface morphology of the NPs was investigated by scanning electron microscopy (SEM) using Zeiss Ultra 55-Limited edition scanning electron microscope. Transmission electron microscope (TEM) images were recorded

using JEM-2100 transmission electron microscope at a working voltage of 200 kV. The NPs were dispersed into ethanol using ultrasonicator for sample preparation for SEM and TEM measurements. A drop of dispersion was placed on the carbon coated grid (300 Mesh) and excess solution was blotted off. The samples were dried at room temperature for 24 hours before the measurement.

## 3. Result and discussion

We herein report a convenient method for the synthesis of $\alpha$-$Fe_2O_3$ nanoparticles (NPs) by simple grinding protocol. Binary mixtures of an ionic liquid (IL), 1-ethyl-3-methylimidazolium ethylsulfate, [$C_2$mim][$C_2OSO_3$] and ethylene glycol (EG) in different mixing ratios have been used as a solvent for precipitation induced formation of $\alpha$-$Fe_2O_3$ NPs. The composition of binary mixture of IL and EG played a vital role in controlling the size and thus in modulation of its various physico-chemical properties. In pure IL, the size of NPs is small with low crystallinity, whereas in pure Ethylene glycol (EG) crystallite size becomes relatively very large. However, the binary mixture of IL and EG played very important role in confining the size of NPs and modifying the optical and magnetic properties of prepared NPs. All the results obtained have been correlated with the nature of the solvent used for the preparation of NPs and discussed one by one.

### 3.1 Structural studies

The XRD patterns of obtained NPs by using different composition of ionic liquid (IL) and ethylene glycol (EG) are shown in Fig.1 (a). The diffraction peaks observed for obtained products matches very well with the hematite (JCPDS card No. 72-0469) indicating the formation of rhombohedral $\alpha$-$Fe_2O_3$ phase (a =5.038 Å, c = 13.772 Å). From the XRD studies, it has been observed that the with the increase in content of IL in IL-EG binary solvent, the crystallinity of obtained NPs decreases as indicated by increase in half line width of the respected diffraction peaks. Here the coordinating nature of the solvent along with their dielectric constant is expected to play an important role in deciding the degree of crystallization and size of the crystallites of NPs. Further, the small peak (012) is quite clear in samples prepared at lower content of IL, however, it seems to be absent in the samples prepared at quite higher concentration of IL. The

reason behind such behavior is supposed to be the decrease in crystallinity of the obtained NPs particles with increase in content of IL in IL-EG binary mixture. Another reason for the absence of (012) peak in αFe-75 and αFe-100 may be the stronger interactions of growing NPs with IL, where the growth of NPs along (012) direction is restricted. The average crystallite size of prepared NPs has been obtained using Scherrer's equation as follows:

$$D = K\lambda / \beta \cos\theta$$

where D is the particle size perpendicular to the normal line of (hkl) plane, *K* is a constant (0.9), $\beta$ is the full width at half-maximum of the (hkl) diffraction peak, θ is the Bragg angle, and λ is the wave-length of X-ray. The variation of obtained size of crystallites as a function of content of IL in IL-EG binary mixture is shown in Fig. 1(b). The size of crystallites for all the prepared NPs lies in the range of 12-47 nm, depending upon the composition of binary mixture of IL and EG. Similar to that of degree of crystallinity, the crystallite size has been found to decrease with increase in content of IL in the IL-EG binary solvent. The crystallite size decreases sharply while moving from *α*Fe-0 to *α*Fe-25 which can be related to change in characteristic properties of the binary solvent. The binary solvent mixtures comprising ILs and other solvent shows completely different physicochemical properties which are not present in the either of the pure solvents [31, 32]. In the IL-EG binary solvent, there exists the dominance of dispersion forces over specific interactions, which increases with increase in content of IL leading to decrease in interactions between constituent ions of IL and EG [31, 32]. This results in enhanced coordinating ability of constituent ions of IL as well as of EG towards different reaction species. During the preparation of $\alpha$-$Fe_2O_3$ NPs, $Fe(OH)_3$ or FeOOH forms as an intermediate after the addition of NaOH as per the following equation:

$$Fe^{3+} + 3OH^- \longrightarrow Fe(OH)_3/FeOOH \xrightarrow{\text{Calcination}} \alpha\text{-}Fe_2O_3$$

Both the EG and constituent ions of IL are expected to interact with $Fe(OH)_3$ and the growing $\alpha$-$Fe_2O_3$ NPs. In the EG-IL binary mixture, at lower content of IL (25 vol %), the ions of IL and EG interacts very strongly with each other [31, 32]. As a consequence of this, constituent ions of IL and EG interact (H-bonding and ion-dipole interactions)

feebly with the $Fe(OH)_3$ leading to their less adsorption on its surface which results in unrestricted growth of NPs. This thereby exerts very less effect on degree of crystallinity during the formation of $\alpha$-$Fe_2O_3$. Further, as the solvent coordinates weekly with the $Fe(OH)_3$, it does not assert the growth of NPs leading to larger size of crystallites at lower content of IL in binary mixture of IL and EG. However, with an increase in content of IL, the interactions between constituent ions of IL and $Fe(OH)_3$ as well as EG and $Fe(OH)_3$ increases at the cost of deceased interactions between IL and EG, where IL acts as a template and thus restricts the growth of crystallites leading to smaller size of NPs. Based on above discussions, a schematic showing the possible mode of interactions between the different components of the reaction mixture is provided as Scheme.2.

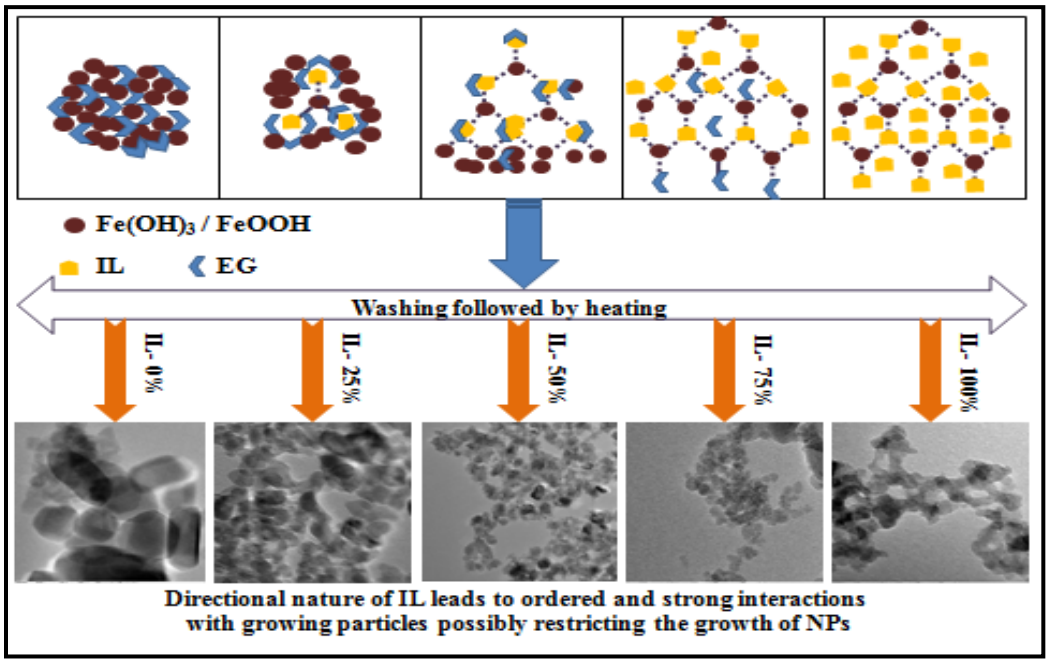


**Scheme.2.** Proposed mechanism for the formation of $\alpha$-$Fe_2O_3$ NPs synthesized in different compositions of IL and EG.

The room temperature Raman spectra of $\alpha$-$Fe_2O_3$ NPs are shown in Fig.2. The Raman bands of obtained NPs have been found to be broadened due to which exact band position could not be located. Further the broadening of the Raman peaks is a common feature of NPs [33]. The three Raman modes for $\alpha$-$Fe_2O_3$ NPs around at 216 ($A_{1g}$), 283 ($E_g$), and 398 ($E_g$) $cm^{-1}$ has been observed, which is in agreement with the literature values [34,

35]. All the Raman bands observed for $\alpha$-$Fe_2O_3$ NPs shifts towards lower wavenumber with increase in content of IL in IL-EG binary mixture with relatively greater shifting in Raman bands present around 283 and 398 $cm^{-1}$. Apart from decrease in size of $\alpha$-$Fe_2O_3$ with increase in content of IL, this shift may be due to interaction of constituent ions of IL interacting with $\alpha$-$Fe_2O_3$ in their crystal lattice. This assumption is well supported by decrease in crystallinity of $\alpha$-$Fe_2O_3$ NPs with increase in IL content. The sample $\alpha$Fe-100 shows very broadened and less intense Raman bands owing to is low crystallinity and smallest size. Thus from Raman and XRD studies, we have concluded that both IL and EG helps in controlling the size and crystallinity of NPs.

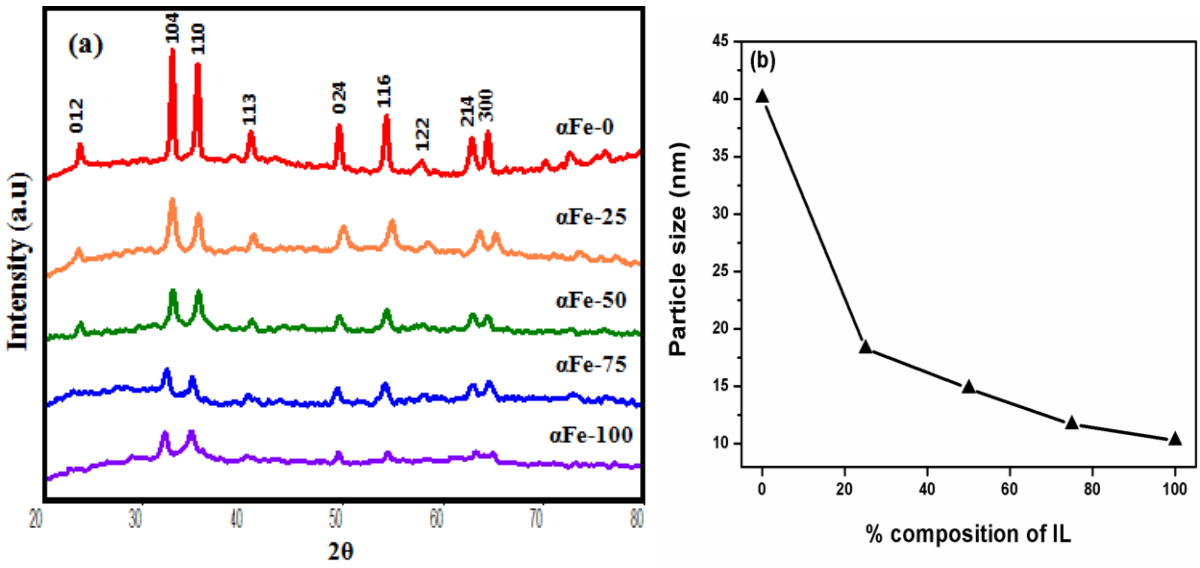


**Fig.1. (a)** XRD spectra of $\alpha$-$Fe_2O_3$ NPs synthesized in binary mixture of IL and EG; and **(b)** variation of particle size as a function of composition of IL-EG binary mixture.

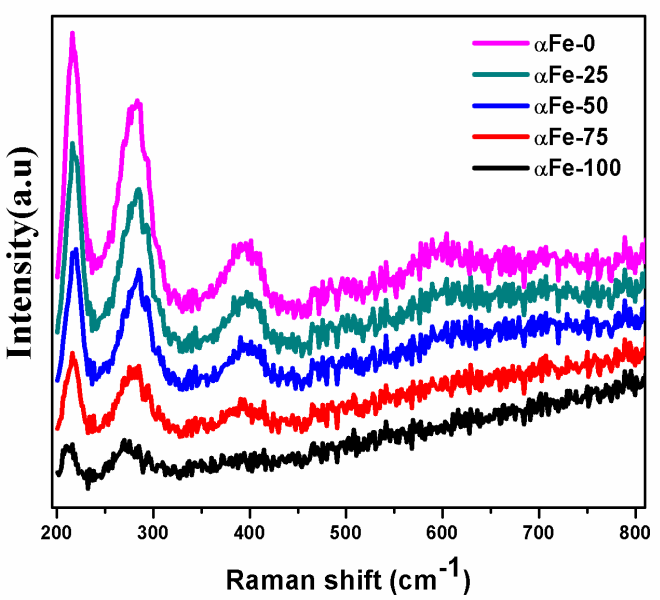


**Fig.2.** Raman spectra of $\alpha$-$Fe_2O_3$ NPs synthesized in binary mixture of IL and EG.

### 3.2 Morphological studies

Morphology and size of the NPs have been characterized by scanning electron microscopy (SEM) and transmission electron microscopy (TEM) techniques and are shown in Fig. 3 and 4, respectively. SEM images indicate that the prepared $\alpha$-$Fe_2O_3$ NPs are roughly spherical in shape. We have not observed any distinct morphological changes for the synthesized NPs from SEM measurements. This indicates that the presence of IL could only affect the size and degree of crystallinity without affecting the morphology of the NPs. Although, the IL 1-ethyl-3-methylimidazolium ethylsulfate has a capability to coordinate with the $Fe(OH)_3$ as an intermediate as well as with the growing NPs, however this small chain IL lacks the amphiphilic character required to control the shape of the NPs by acting as structure directing template. It can be seen from the SEM images that with increase in content of IL in binary solvent, the size of the NPs decreases corroborating with the XRD results. The NPs obtained from lower content of IL ($\alpha$Fe-0 to $\alpha$Fe-50) are appear to be more disperse than those obtained from higher content of IL ($\alpha$Fe-75 and $\alpha$Fe-100) which shows some aggregation with decrease in particle size and this type of behavior also seen in TEM studies. The IL exhibits lower surface tension as compared to that of water, thus resulting in high nucleation rate than the growth rate, which helps in formation of relatively smaller NPs [29, 36]. Here the role of polarity and

viscosity of solvent in controlling the size of NPs is as important as the coordination of constituents of binary solvent with $Fe(OH)_3$ in deciding the size and crystallinity of NPs. The polarity and viscosity of IL-EG binary mixture decreases and increases respectively, with increase in content of IL. A decrease in polarity is expected to enhance the aggregation, whereas an increase in viscosity is assumed to decrease the extent of aggregation of NPs. A decrease in size of the NPs with increase in content of IL thus indicates that the size of the NPs are being controlled by the viscosity factor as a dominating one along with the enhanced coordination of the constituents of binary solvents with the NPs with increase in content of IL.

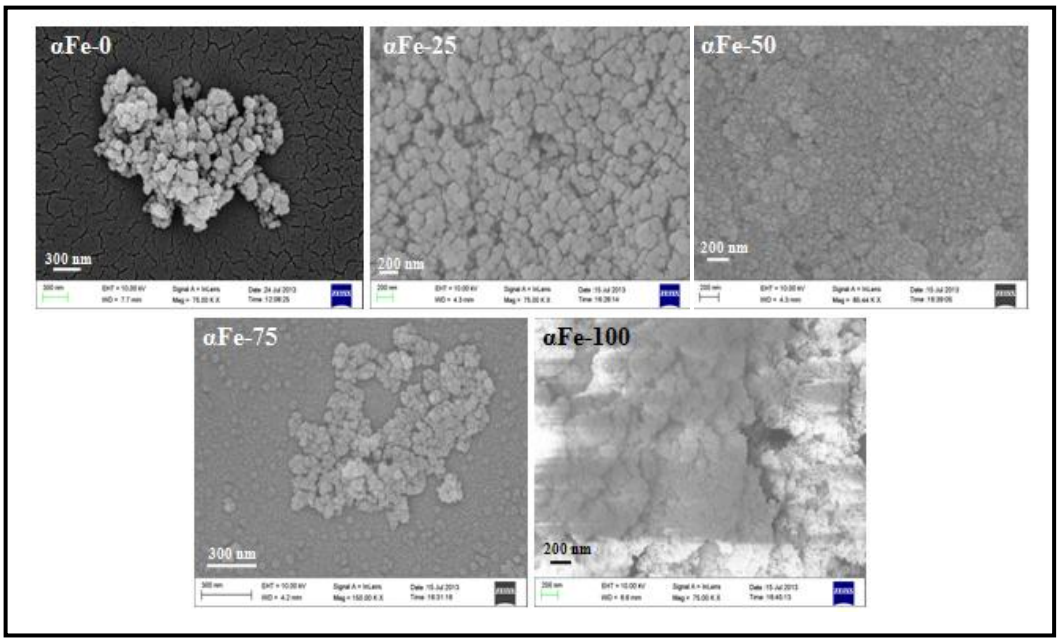


**Fig.3.** SEM images of α-$Fe_2O_3$ NPs synthesized using different compositions of IL-EG binary mixture.

As can be seen from Fig. 4, TEM images strongly support the observation made by SEM measurements. As we move from *α*Fe-0 to *α*Fe-100, a decrease in particle size has been observed in corroboration with the results obtained from XRD and SEM measurements. The *α*Fe-0 NPs have been found to be a mix of near spherical to rectangular in shape (20-40 nm). The NPs obtained for *α*Fe-25 are near spherical in shape (14-19 nm), whereas NPs obtained as *α*Fe-50 (10-15 nm) don't reveal any specific morphology. With further

increase in content of IL i.e. for $\alpha$Fe-75, agglomerated NPs with near spherical shape (6-10 nm) have been observed indicating the effect of composition of binary solvent mixture on shape of the NPs. Very surprisingly, in neat IL, the formed NPs ($\alpha$Fe-100) adopted an interconnected network of NPs (7-11 nm) having a hollow space between interconnections. Although the IL is homogeneous macroscopically, however the existence of nano-segregation even in small chain ILs, where polar and non-polar domains are separated microscopically is a well established phenomenon [37]. It seems that the IL and the intermediate i.e. $Fe(OH)_3$ forms a complex structure where $Fe(OH)_3$ arranges itself in a way similar to core-shell structure having IL in the core and $Fe(OH)_3$ at the periphery. The hydrogen-bonding interactions between sulfate anion of IL and hydroxyl group of $Fe(OH)_3$ are assumed to be responsible for stabilization of such type of structures. The washing of the final product after calcinations removes the IL trapped inside the network of formed $\alpha$-$Fe_2O_3$ NPs leading to formation of nanoholes. The SAED pattern (as shown in the inset of TEM images) supports the extent of crystallinity of $\alpha$-$Fe_2O_3$ NPs obtained in different binary solvent mixtures. The SAED pattern shows concentric rings along with some spots thus indicating the polycrystalline nature of the prepared samples. However, in case of NPs obtained at high content of IL in binary mixture ($\alpha$Fe-50 to $\alpha$Fe-100), a clear diffraction pattern has not been observed. Further, the reduced number of diffraction rings for the NPs obtained from higher content of IL ($\alpha$Fe-75, $\alpha$Fe-100) may indicates the decrease in crystallinity of obtained NPs and thus can be corroborated with the XRD measurements.

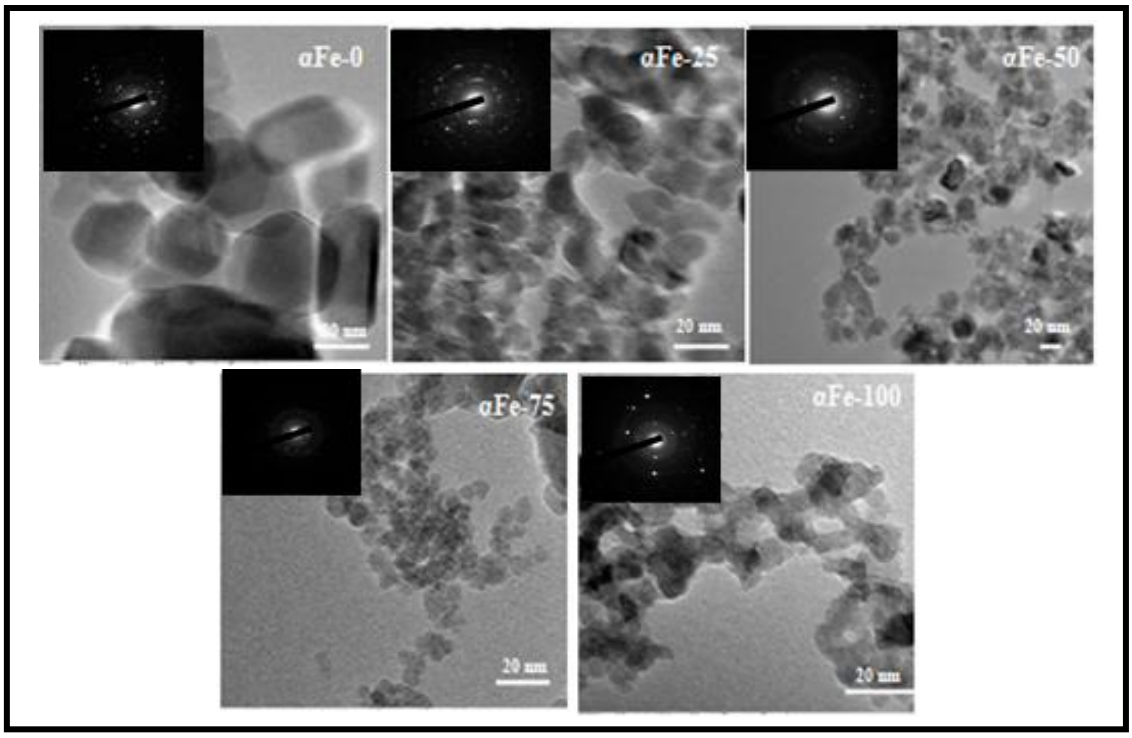


**Fig.4.** TEM images of $\alpha$-$Fe_2O_3$ NPs synthesized using different compositions of IL and EG. (SAED pattern shown in inset)

**Table.1.** Physico-Chemical parameters of $\alpha$-$Fe_2O_3$ NPs obtained from binary mixture of IL-EG.

| Sample | Average particle size from XRD (nm) | Particle size from TEM (nm) | Saturation Magnetization (emu/g) | Remnant Magnetization (emu/g) | Coercivity (Oe) |
|---|---|---|---|---|---|
| 0 | 40.1 | 20-40 | 9.03 | 0.023 | 1.57 |
| 25 | 18.3 | 14-19 | 2.27 | 0.020 | 7.12 |
| 50 | 14.8 | 10-15 | 4.88 | 0.002 | 0.39 |
| 75 | 11.7 | 6-10 | 8.51 | 0.003 | 0.58 |
| 100 | 10.3 | 7-11 | 10.27 | 0.097 | 21.5 |

### 3.3 UV-Vis studies

The optical absorption properties of NPs are greatly dependent on particle size and shape and to explain this behavior, UV-Vis spectra have been recorded for the synthesized $\alpha$-

$Fe_2O_3$ NPs and are shown in Fig 5. The synthesized NPs show an absorption band around 210-225 nm region in UV region and a broad band spanning between 400-600 nm in visible region. The band in the visible region seems to be comprised of two sub-bands i.e. a band at 400 and 600 nm. The main contribution of optical absorption spectra of $Fe^{3+}$ containing substances are d-d transition, ligand to metal charge-transfer transition and the simultaneous excitations of two neighboring $Fe^{3+}$ cations that are magnetically coupled *i.e.* pair excitations [38]. The variation in absorbance maxima for band around 400 nm is much clearer than that for band around 600 nm when compared for $\alpha$-$Fe_2O_3$ NPs obtained from different binary mixtures. The band at around 400 nm shows a significant blue shift while going form $\alpha$Fe-0 (410 nm) to $\alpha$Fe-50 (375 nm) due to decrease in particle size, whereas surprisingly again a red shift has been observed while going from $\alpha$Fe-50 to $\alpha$Fe-100. This red shift can be explained on the basis of development of surface stress [39] due to greater reduction in particle size by increase in the content of IL in binary mixture. The UV spectra reveals that NPs obtained from different IL-EG binary mixtures have different photo-physical properties which can be related to size, crystallinity and state of aggregation in NPs.

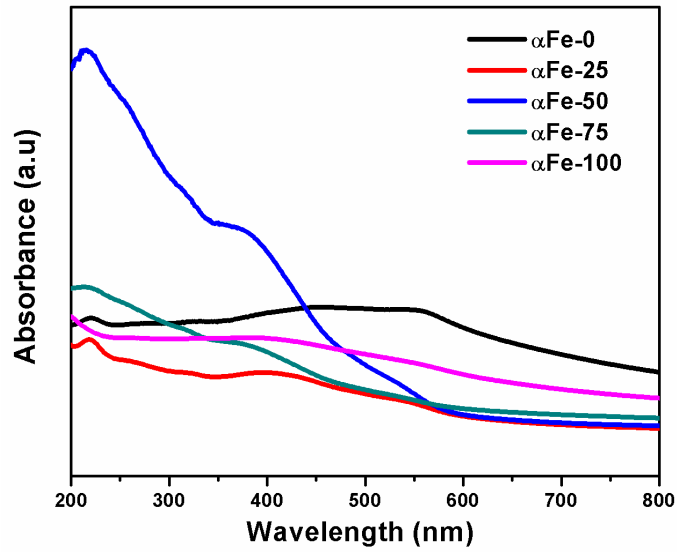


**Fig.5.** UV-Vis spectra of $\alpha$-$Fe_2O_3$ NPs synthesized using different compositions of IL and EG

### 3.4 Photoluminescence studies

Photoluminescence spectra of prepared $\alpha$-$Fe_2O_3$ NPs are shown in Fig. 6 (a) and (b) where strong photoluminescence confirm their emitting nature. In bulk, $\alpha$-$Fe_2O_3$ does not

show photoluminescence due to the local forbidden d–d transition, resonant energy transfer between cations and efficient lattice and magnetic relaxations [40]. However hematite nanostructures show photoluminescence due to quantum confinement effect, which results in delocalization and quantization of electronic state [41]. At an excitation wavelength of 390 nm, the $\alpha$-$Fe_2O_3$ NPs shows an intense emission band around 587 nm and a weak emission band at 525 nm, whereas at excitation wavelength of 450 nm, an emission band around 675 nm has been observed. The origin of luminescence in $\alpha$-$Fe_2O_3$ NPs can be attributed to the decrease in particle size which leads to the reduction in magnetic interactions as compared to that in bulk due to loss of ferromagnetic long range order. The change in the density of electronic population of valence band also enhanced electron-phonon coupling [42-44]. The inset of Fig. 6(a) shows the variation in intensity of emission band around 587 nm for NPs prepared in different binary solvents as a function of content of IL in IL-EG binary mixture. The emission intensity increases while going from $\alpha$Fe-0 to $\alpha$Fe-50, while it decreases moving beyond $\alpha$Fe-50 towards $\alpha$Fe-100. At lower content of IL (0-50%), as discussed in earlier sections, constituent ions of IL don't coordinate efficiently with $Fe(OH)_3$ and hence with forming $\alpha$-$Fe_2O_3$ crystallites, thereby exerting no effect on photophysical properties of $\alpha$-$Fe_2O_3$ NPs. The enhancement in emission intensity can be related to dominance of decrease in size of NPs. However at higher content of IL, despite a decrease in size of NPs, the emission intensity decreases. At such high concentrations of IL, there is dominance of increased coordination of constituent ions of IL with forming $\alpha$-$Fe_2O_3$ crystallites leading to surface modification where IL ions may remain coordinated after formation of $\alpha$-$Fe_2O_3$ NPs. The presence of ions of IL may lead to enhanced lattice and magnetic relaxation leading to decrease in emission intensity at higher content of IL. Similar behavior has been observed while analyzing the emission intensity obtained at an excitation wavelength of 450 nm as can be seen from Fig. 6(b). This observation can be correlated with variation in hyperfine field (discussed in Mössbauer section) which first decreases upto $\alpha$Fe-50 and then increases thus results in the variation of emission intensity. This reduction of hyperfine field for $\alpha$Fe-50 as compared to others may leads to enhancement of its emission intensity [44]. Further, the emission spectra shown by different NPs are red shifted as compared to

that observed for $\alpha$Fe-0. This can be due to surface modification of NPs by the constituent ions of IL.

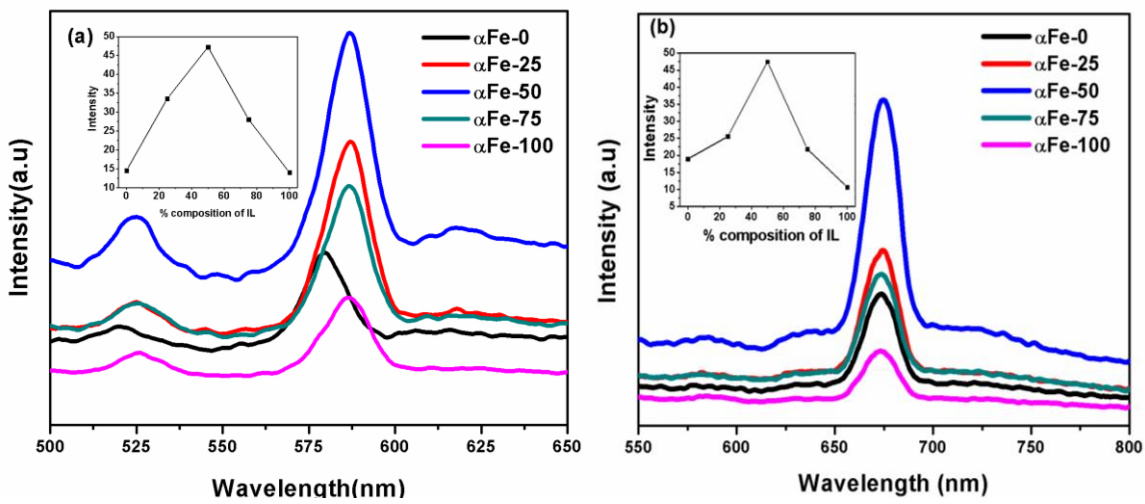


**Fig .6.** Photoluminescence spectra of $\alpha$-$Fe_2O_3$ NPs [$\lambda_{exc}$= (a) 390 nm and (b) 450 nm].

### 3.5 Mössbauer analysis

Fig.7. shows the room temperature Mössbauer spectra of $\alpha$-$Fe_2O_3$ NPs obtained from the different compositions of binary mixture of IL and EG at the room temperature. The detailed values of Mössbauer spectral parameters of $\alpha$-$Fe_2O_3$ NPs are summarized in Table.2. For the Mössbauer spectra of $\alpha$Fe-0, a six line hyperfine pattern has been observed similar to that of bulk $\alpha$-$Fe_2O_3$. For $\alpha$Fe-25 also, a sextet pattern has been observed, but with a minor asymmetry as compared to $\alpha$Fe-0. The isomer shift of 0.378 and 0.346 mm/s with magnetic hyperfine field of 51.6 and 51.05 T displayed by $\alpha$Fe-0 and $\alpha$Fe-25, respectively, shows a close match with reported values for hematite [45]. The presence of central quadrupole doublet along with sextet in the spectra of $\alpha$Fe-50, $\alpha$Fe-75 and $\alpha$Fe-100 can be attributed to the superparamagnetic nature of these NPs [46-48]. As the composition of IL above 25%, an appearance of central doublet in the spectra along with less intense sextet which is a typical behavior for magnetic NPs exhibiting superparamagnetic relaxation [49,50]. The chemical environment of Fe nuclei may change due to different extent of interaction of growing NPs with IL and EG at different compositions of binary solvent mixture which affects the magnetic properties of prepared NPs. The broadened sextet and duplet in the Mössbauer spectra of $\alpha$Fe-50 has been

observed with lower $B_{HF}$ value (47.1T) which can be attributed to small size and dispersed nature of these particles as indicated more clearly from SEM image. This indicates the reduction in magnetic interactions which are also well supported by increase in absorption and emission intensity of $\alpha$Fe-50 in UV and PL studies, respectively. For sample $\alpha$Fe-75 there is a slight increase in $B_{HF}$ (48.75 T) and for $\alpha$Fe-100 it again increase to somewhat large extent (51.36 T) inspite of its comparable particle size with $\alpha$Fe-75. This behavior is also supported from magnetic studies where increase in $M_S$ has been observed from $\alpha$Fe-50 to $\alpha$Fe-100 (Discussed in next section). Such behavior can be explained on the basis that for $\alpha$Fe-100, the IL may interacts more with the surface of the growing particles than inside of growing particles, which interact ferromagnetically due to strong interparticle interaction and thus may be responsible for the increased $M_S$ and $B_{HF}$ value. The other possibility may be the lattice strain in small sized particles which is supported by a red shift of low intensity in UV spectra. Therefore it is observed that apart from controlling the size, shape and optical properties of $\alpha$-$Fe_2O_3$ NPs, the composition of binary solvent mixture also controls the magnetic properties of $\alpha$-$Fe_2O_3$ NPs where transformation of ferromagnetic ($\alpha$Fe-0, and $\alpha$Fe-25) to superparamagnetic ($\alpha$Fe-50, $\alpha$Fe-75 and $\alpha$Fe-100) character has been observed.

**Table.2.** Mössbauer parameters of $\alpha$-$Fe_2O_3$ NPs recorded at room temperature.

| Sample | IS* (mm/s) | QS (mm/s) | BHF (T) | Spectral area (%) |
|---|---|---|---|---|
| $\alpha$Fe-0 | 0.378 | - | 51.38 | 100 |
| $\alpha$Fe-25 | 0.346 | - | 51.05 | 100 |
| $\alpha$Fe-50 | S= 0.341<br>D= 0.372 | -<br>0.808 | 47.1<br>- | 55<br>45 |
| $\alpha$Fe-75 | S= 0.408<br>D= 0.383 | -<br>0.786 | 48.75<br>- | 27<br>73 |
| $\alpha$Fe-100 | S= 0.373<br>D= 0.364 | -<br>0.707 | 51.36<br>- | 18<br>82 |

* w.r.t pure iron absorber, S=sextet, D=central doublet

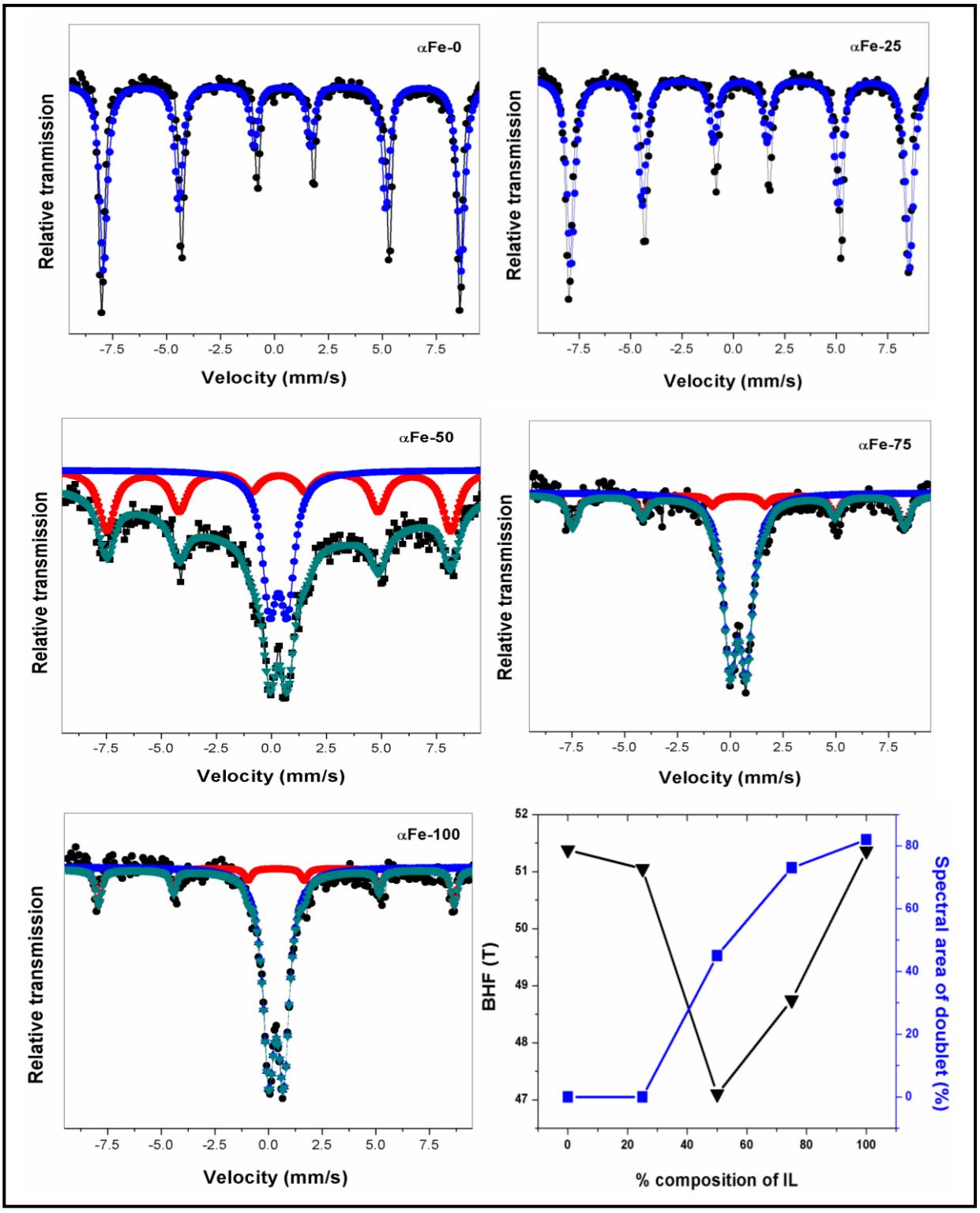


**Fig.7.** Mössbauer spectra of $\alpha$-$Fe_2O_3$ NPs synthesized by using different composition of IL-EG binary mixture.

### 3.6 Magnetic Studies

Magnetic properties of $\alpha$-$Fe_2O_3$ prepared NPs were carried out at room temperature. In general, $\alpha$-$Fe_2O_3$ shows antiferromagnetic nature below Morin temperature ($T_M$ = 263K) and can exhibit weak ferromagnetic behavior between 263K ($T_M$) and 960K *i.e.* at Neel temperature ($T_N$) due to slight canting of spin above $T_M$ [51]. Fig.8. shows the magnetic hysteresis loops of $\alpha$-$Fe_2O_3$ NPs, which are indicative of weak ferromagnetic nature of NPs. All types of prepared NPs using different IL-EG binary mixtures show negligible remnant magnetization ($M_r$) and coercivity ($H_c$), thus indicating the superparamagnetic nature of NPs (Table.1). The remnant magnetization ($M_r$) and coercivity ($H_c$) of obtained NPs are less as compared to that reported in literature [52] indicating the presence of superparamagnetism in prepared NPs. The saturation magnetization obtained for synthesized NPs lies in the range of 2.27-10.27 emu/g depending upon the composition of IL and EG in the binary mixture. The saturation magnetization decrease initially ($\alpha$Fe-0 to $\alpha$Fe-25) followed by an increase ($\alpha$Fe-50 - $\alpha$Fe-100) as shown in Fig.9. It is well known that magnetic properties of ferromagnetic materials are greatly influenced by morphologies and structure of NPs [53]. As the size of $\alpha$-$Fe_2O_3$ particles approaches to nanometer scale, due to the nanoscale confinement [54], unusual magnetic behavior has been observed. This behavior is quite different from those of conventional bulk materials (antiferromagnetic at low temperature and ferromagnetic above $T_M$). When particle becomes small enough, the magnetic moment in a single domain fluctuates in a certain direction due to thermal agitation, leading to superparamagnetic behavior above the blocking temperature ($T_B$) [55]. The increase in the content of IL in the binary mixture leads to decrease in size of NPs. This decrease in size enhances the contribution of uncompensated surface spins and the NPs tend to interact ferromagnetically. Such interactions may lead to enhancement of $M_s$. The obtained $M_s$ value for the NPs are higher than as reported by Zheng *et al*. [23, 26] which can be attributed to small sized NPs resulting in dominance of uncompensated surface spins. Further, the magnetization of smaller NPs randomly flips due to thermal fluctuations which exhibits enhanced magnetization in an external magnetic field and shows the behavior of superparamagnetics [56, 57]. Thus with increase in the content of IL, the sample $\alpha$Fe-100 shows greater essence of superparamagnetism with enhanced $M_s$. This observation has

also been confirmed from the Mössbauer studies where the spectral area of doublet increases along with increase in $B_{HF}$ for $\alpha$Fe-100. The $\alpha$Fe-0 and $\alpha$Fe-25 NPs also show negligible $M_r$ and $H_c$ like other samples. But the Mössbauer spectra shows only sextet which may be due to shorter time scale for Mössbauer measurements than magnetic measurements. According to Neel–Brown theory, the temperature also affects the superparamagnetic relaxation times [58, 59]. The super-paramagnetic relaxation time may be in the picoseconds range when the thermal energy is comparable to or larger than the magnetic anisotropy energy. In that case, the main sextet signal is dominant inspite of superparamagnetic signal which might be present in the spectrum. Another possibility for such behavior where superparamagnetic nature has not observed may be based on the particle size distribution in the sample. The smallest particles in the sample have a much lower Debye–Waller factor than the larger particles, resulting in non-observation of superparamagnetic doublet from the smaller particles compared to that of sextet signal from the larger particles in Mössbauer spectrum [60]. Some reports are also available in literature where superparamagnetic (doublet) signal is not observed even though the magnetic studies show superparamagnetic nature [61, 62]. The $\alpha$Fe-0 also shows higher $M_S$ (9.03emu/g) which is comparable with $\alpha$Fe-100 (10.27emu/g). The possible reasons for such behavior can be the reduction of some $Fe^{3+}$ to $Fe^{2+}$ in neat EG, due to weak reducing action of EG, which results in the appearance of ferromagnetic like character due to non-cancellation of spins. Thus superparamagnetic nature of prepared NPs provides a new pathway, particularly in applications where superparamagnetic behavior is advantageous over ferromagnetic behavior [63].

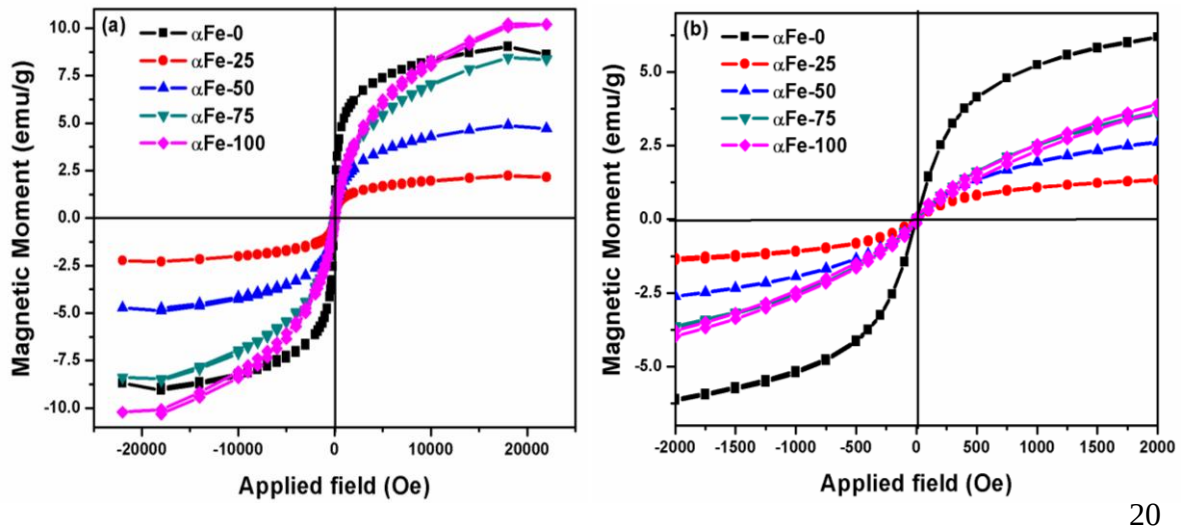

**Fig.8.(a)** Hysteresis loop of α-$Fe_2O_3$ NPs synthesized in binary mixture of IL and EG and **(b)** enlarged view of Fig. 8 (a) in the lower range of applied field.

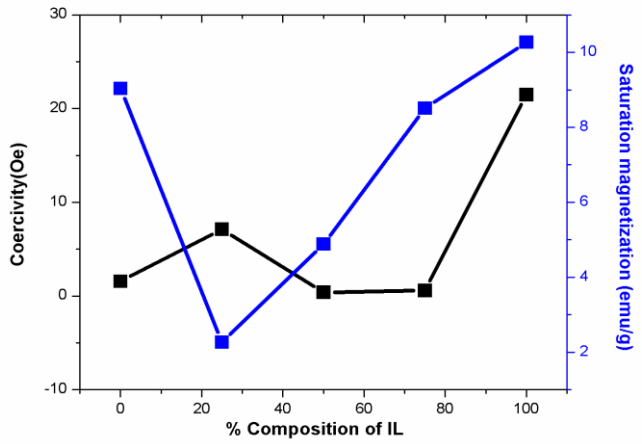


**Fig.9.** Variation of $H_c$ and $M_S$ for the NPs obtained from different compositions of IL and EG.

## Conclusion

The $\alpha$-$Fe_2O_3$ nanoparticles (NPs) have been synthesized by a facile, convenient, effective and fairly low temperature route in the binary mixture of ionic liquid (IL) and ethylene glycol (EG). The characteristic properties of NPs such as crystallinity, size, magnetic and luminescent properties have been found to be dependent on the composition of binary mixture of IL and EG. A decrease in particle size along with decrease in crystallinity of NPs with increase in content of IL has been observed. The $\alpha$-$Fe_2O_3$ NPs prepared in different binary solvent mixtures exhibits weak ferromagnetic character, whereas, the NPs prepared exclusively in binary solvent having higher content of IL (50, 75 and 100 %) have shown superparamagnetic character which goes on increasing with increase in the amount of IL. This modulation from weak ferromagnetic to superparamagnetic phase along with luminescent character of the synthesized NPs makes its possible as a good candidate for targeting/delivering specific molecules in living cell under the magnetic field by using a fluorescent microscope in biomedical applications.

**Acknowledgement**

The authors are very thankful to the Defence Research and Development Organization (DRDO), New Delhi, India for financial support.

**References**

[1] N. Pailhé, A. Wattiaux, M. Gaudon and A. Demourgues, *J. Solid State Chem.*, 2008, **181**, 2697–2704.

[2] L. Huo, W. Li, L. Lu, H. Cui, S. Xi, J. Wang, B. Zhao, Y. C. Shen and Z. Lu, *Chem. Mater.*, 2000, **12**, 790–794.

[3] Z. Y. Fan, X. G. Wen, S. H. Yang and J. G. Lu, *Appl. Phys. Lett.*, 2005, **87**, 0131131–0131133.

[4] A. Kay, I. Cesar and M. Gratzel, *J. Am. Chem. Soc.*, 2006, **128**, 15714–15721.

[5] I. Cesar, A. Kay, J. A. G. Martinez and M. Gratzel, *J. Am. Chem. Soc.*, 2006, **128**, 4582–4583.

[6] A.K. Gupta and M. Gupta, *Biomaterials* 2005, **26**, 3995–4021.

[7] T. Ninjbadgar, S. Yamamoto and T. Fukuda, *Solid State Sci.*, 2004, **6**, 879–885.

[8] A. Watanabe and H. Kozuka, *J. Phys. Chem. B* 2003, **107**, 12713–12720.

[9] S. Wagloehner, D. Reichert, D.L. Sorzano, P. Balle, B. Geiger and S. Kureti, *J. Catal.*, 2008, **260**, 305–314.

[10] A. D. Wheeler, G. Wang, Y. Ling, Y. Li and J. Z. Zhang, *Energy Environ. Sci.*, 2012, ***5***, 6682-6702.

[11] C. Y. Cao, J. Qu, W. S. Yan, J. F. Zhu, Zi. Y. Wu, and W. G. Song, *Langmuir* 2012, **28**, 4573−4579.

[12] L. Liu, H. Z. Kou, W. Mo, H. Liu and Y. Wang, *J. Phys. Chem. B* 2006, **110**, 15218-15223.

[13] M. Sorescu, R. A. Brand, D. M. Tarabasanu and L. Diamandescu, *J. Appl. Physics.*, 1999, **85**, 5546-5548.

[14] X. C. Jiang, A. B. Yu, W. R. Yang, Y. Ding, C. X. Xu and S. Lam, *J. Nanopart. Res.*, 2010, **12**, 877–893.

[15] S. B. Wang, Y. L. Min and S. H. Yu, *J. Phys Chem. C* 2007, **111**, 3551-3554.

[16] D. Dorjnamjin, M. Ariunaa and Y. K. Shim, *International Journal of Molecular Sciences* 2008, **9**, 807-820.

[17] J. Dupont, G. S. Fonseca, A. P. Umpierre, P. F. P. Fichtner, and S. R. Teixeira, *J. Am. Chem. Soc.*, 2002, **124**, 4228-4229.

[18] D. P. Liu, G. D. Li, Y. Su and J. S. Chen, *Angew. Chem., Int. Ed.* 2006, ***45***, 7370–7373.

[19] E. R. Cooper, C. D. Andrews, P. S. Wheatley, P. B. Webb, P. Wormald and R. E. Morris, *Nature* 2004, **430**, 1012–1016.

[20] B. G. Trewyn, C. M. Whitman and V. S. Y. Lin, *Nano Lett.*, 2004, ***4***, 2139–2143.

[21] S. W. Cao and Y. J. Zhu, *Acta Mater.*, 2009, ***57***, 2154–2165.

[22] W. J. Zheng, X. D. Liu, Z. Y. Yan and L. J. Zhu, *ACS Nano* 2009, **3**, 115–122.

[23] J. Lian, X. Duan, J. Ma, P. Peng, T. Kim, and W. Zheng, *ACS Nano* 2009, **3**,3749–3761.

[24] C. M. Lee, H. J. Jeong, S. T. Lim, M. H. Sohn, and D. W. Kim, ACS *Appl. Mater. Interfaces* 2010, **2**, 756–759.

[25] L. Xu, J. Xia, L. Wang, J. Qian, H. Li, K. Wang, K. Sun, and M. He, *Chem. Eur. J.*, 2014, **20**, 2244 – 2253.

[26] J. Ma, T. Wang, X. Duan, J. Lian, Z. Liu and W. Zheng *Nanoscale.*, 2011, **3**, 4372-4375.

[27] J. Ma, J. Teo, L. Mei, Z. Zhong, Q. Li, T. Wang, X. Duan, J. Lianc and W. Zheng, *J. Mater. Chem.*, 2012, **22**, 11694-11700.

[28] L. Xu, J. Xia, K. Wang, L. Wang, H. Li, H. Xu, L. Huangb and M. He, *Dalton Trans.*, 2013, **42**, 6468-6477.

[29] M. Antonietti, D. Kuang, B. Smarsly and Y. Zhou, *Angew. Chem., Int. Ed.* 2004, **43**, 4988–4992.

[30] A. Mele, C. D. Tran and S. H. D. Lacerda, *Angew. Chem. Int. Ed.*, 2003, **42**, 4364 – 4366.

[31] T. Singh, K. S. Rao and A. Kumar, *Chem Phys Chem.*, 2011, **12**, 836 – 845.

[32] T. Singh, A. Kumar, M. Kaur, G. Kaur and H. Kumar, *J. Chem. Thermodynamics.*, 2009,41, 717–723.

[33] W. B. White, *J. Ceram. Process Res.*, 2005, **6**, 1-9.

[34] K. V. Manukyan, Y. S. Chen, S. Rouvimov, P. Li, X. Li, S. Dong, X. Liu, J. K. Furdyna, A. Orlov, G. H. Bernstein, W. Porod, S. Roslyakov and A. S. Mukasyan, *J. Phys. Chem. C.,* 2014, **118**, 16264−16271.

[35] H. M. Fan, G. J. You, Y. Li, Z. Zheng, H. R. Tan, Z. X. Shen, S. H. Tang and Y. P. Feng, *J. Phys. Chem. C* 2009, **113**, 9928–9935.

[36] X. D. Liu, J. M. Ma, P. Peng, W. J. Zheng, *Mater. Sci. Eng. B.*, 2008, **150**, 89–94.

[37] K. Shimizu, C. E. S. Bernardes, A. Triolob and J. N. C. Lopes, Phys. Chem. Chem. Phys., 2013, **15**, 16256-16262.

[38] Y. P. He, Y. M. Miao, C. R. Li, S. Q. Wang, L. Cao, S. S. Xie, G. Z. Yang, B. S. Zou, C. Burda, *Phys. Rev. B* 2005, **71**, 125411–125420.

[39] J. K. Vassiliou, V. Mehrotra, M. W. Russell, E. P. Giannelis, R. D. McMichael, R. D. Shull, and R. F. Ziolo, *J. Appl. Phys.*, 1993, **73**, 5109-5116.

[40] N. Tsuda, K. Nasu, A. Yanase and K. Siratori, Edited by M. Cardona, *Electronic Conduction in Oxide* (Springer Series in Solid State Science 94), Springer-Verlag, Berlin, 1991.

[41] S. H. Tolbert and A. P. Alivisatos, *Science* 1994, **265**, 373–376.

[42] B. Zou, W. Huang, M. Han, S.F.Y. Li, X. Wu, Y. Zhang, J. Zhang, P. Wu and R. Wang, *J. Phys. Chem. Sol.*, 1997, **58**, 1315-1320.

[43] B. Zou, G. Tang, G. Zhang and W. Chen, *Acta Phys. Sinica.*, 1993, **42** 1127-1133.

[44] P. Ayyub, M. Mullani, M. Barma, R. Palkar and R. Bijayaraghavan, *J. Phys. C* 1988, **21**, 2229-2245.

[45] L. C. Sanchez, J. D. Arboleda, C. Saragovi, R. D. Zysler and C. A. Barrero, *Physica B.*, 2007, **389**, 145–149.

[46] W. Kündig and H. Bömmel, *Phys. Rev.*, 1966, **142**, 327-332.

[47] B. Ganguly, F. E. Huggins, R. P. M. Rao and G. P. Huffman, *J. Catalysis.*, 1993, **142**, 552-560.

[48] C. Frandsen and S. Mørup, *J. Magn. Magn. Mater.*, 2003, **266**, 36-48.

[49] J. G. Kim, K. H. Han, C. H. Lee and J. Y. Jeong, *Journal of the Korean Physical Society.*, 2001, **38**, 798-802.

[50] S. Mukherjee, D. Das, S. Mukherjee and P.S. Chakrabati, *J.Phys.Chem.C,* 2010, **114** 14763–14771.

[51] X. M. Liu, S. Y. Fu, H. M. Xiao and C. J. Huang, *J. Solid State Chem.*, 2005, **178,** 2798.

[52] X. Wang, L. Zhang, Y. Ni, J. Hong and X. Cao, *J. Phys. Chem. C* 2009**, 113**, 7003–7008.

[53] M. Sorescu, R. A. Brand, D. M. Tarabasanu and L. Diamandescu, *J. Appl. Phys.*, 1999, **85**, 5546–5548.

[54] H. Arnim, Chem. Rev., 1989, **89**, 1861-1871.

[55] M. Tadić, D. Marković , V. Spasojević , V. Kusigerski, M. Remškar, J. Pirnat and Z. Jagličić, *J. Alloys Compd.*, 2007, **441**, 291-296.

[56] B. Martínez, X. Obradors, L. Balcells, A. Rouanet and C. Monty, *Phys. Rev. Lett.*, 1998, **80**, 181−184.

[57] A. -H. Lu, E. L. Salabas and F. Schüth, Angew. Chem., Int. Ed. Engl., 2007, **46**, 1222−1244.

[58] L. Neel, Ann. Geophys., 1949, **5**, 99–136.

[59] W.F. Brown Jr., *Phys. Rev.*, 1963, **130**, 1677–1686.

[60] R. Alcántara, P. Lavela. G. Ortiz, I. Rodríguez and J. L. Tirado, *Hyperfine Interactions.*, 2008, **187**, 13–17.

[61] S. Morup, H. Topsoe, *Appl. Phys.*, 1976, **11** 63–66.

[62] M. F. Hansen, F. Bødker, S. Mørup, K. Lefmann, K. N. Clausen and P. -A. Lindgard, *Phys. Rev. Lett.*, 1997, **79**, 4910–4913

[63] S. K. Suh, K. Yuet, D. K. Hwang, K. W. Bong, P. S. Doyle and T. A. Hatton, *J. Am. Chem. Soc.*,2012, **134**, 7337−7343.

## Table of contents

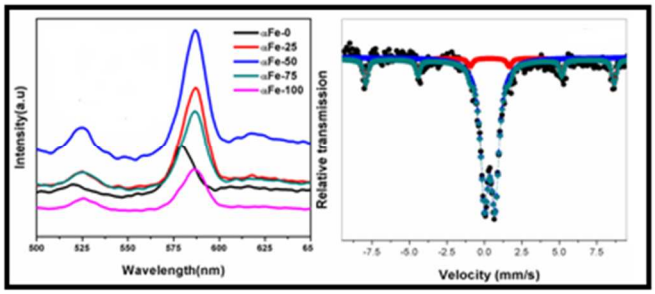


The composition of IL and EG binary solvent mixture affects the structural, morphological, luminescent and magnetic properties of $\alpha$-$Fe_2O_3$ nanoparticles.